

Higher-order theories and radial basis functions applied to free vibration analysis of thin-walled beams

*Original*

Higher-order theories and radial basis functions applied to free vibration analysis of thin-walled beams / Pagani, Alfonso; Carrera, Erasmo; Ferreira, A. J. M.. - In: MECHANICS OF ADVANCED MATERIALS AND STRUCTURES. - ISSN 1537-6494. - STAMPA. - 23:9(2016), pp. 1080-1091. [10.1080/15376494.2015.1121555]

*Availability:*

This version is available at: 11583/2588178 since: 2016-09-12T14:45:59Z

*Publisher:*

Taylor & Francis

*Published*

DOI:10.1080/15376494.2015.1121555

*Terms of use:*

This article is made available under terms and conditions as specified in the corresponding bibliographic description in the repository

*Publisher copyright*

(Article begins on next page)

# Higher-order Theories and Radial Basis Functions Applied to Free Vibration Analysis of Thin-Walled Beams

A. Pagani<sup>1\*</sup>, E. Carrera<sup>1,2†</sup>, A.J.M. Ferreira<sup>3,4‡</sup>

<sup>1</sup>Department of Mechanical and Aerospace Engineering, Politecnico di Torino,  
Corso Duca degli Abruzzi 24, 10129 Torino, Italy.

<sup>2</sup>School of Aerospace, Mechanical and Manufacturing Engineering,  
RMIT University, Bundoora VIC 3083, Australia.

<sup>3</sup>Faculdade de Engenharia da Universidade do Porto, Porto, Portugal.

<sup>4</sup>King Abdulaziz University, Jeddah, Saudi Arabia.

Submitted to:

**Mechanics of Advanced Materials and Structures,**

Special Issue dedicated to Carrera Unified Formulation

*Author for correspondence:*

A. Pagani, Ph.D. Student,  
Department of Mechanical and Aerospace Engineering,  
Politecnico di Torino,  
Corso Duca degli Abruzzi 24,  
10129 Torino, Italy,  
tel: +39 011 090 6870  
fax: +39 011 090 6899  
e-mail: alfonso.pagani@polito.it

---

\*PhD Student, e-mail: alfonso.pagani@polito.it

†Full Professor, e-mail: erasmo.carrera@polito.it

‡Full Professor, e-mail: ferreira@fe.up.pt

## ***Abstract***

*In this paper, the efficiency of the radial basis functions (RBFs) method when applied to higher-order beam theories is investigated. The displacement field of the generic-order beam model is expressed by making use of the Carrera Unified Formulation (CUF). The strong form of the Principle of Virtual Displacements (PVD) is used to obtain the equations of motion of beams in free vibration. The hierarchical capability of the CUF, in conjunction with the PVD, allows to write the governing equations and the natural boundary conditions in terms of fundamental nuclei. The nuclei can be automatically expanded depending on the theory order  $N$ , which is a free parameter of the formulation. Locally supported Wendland's  $C^6$  radial basis functions are subsequently used to approximate the derivatives of the generalized displacements, which are collocated on a number of points (centers) along the beam axis. Several numerical results are proposed including solid structures as well as open and closed thin-walled sections. The solutions by the proposed method are compared both by published literature and by solid/shell models from the commercial code MSC Nastran.*

**Keywords:** Radial basis functions; Unified formulation; Free vibration; Higher-order theories; Beams

# 1 Introduction

Vibration of slender bodies is an important topic in the design of aerospace, mechanical, and civil applications. The majority of classical theories, such as the Euler-Bernoulli beam model (EBBM) [1], usually neglect the transverse shear and the rotatory inertia. EBBM yields reasonably good results when slender, solid, homogeneous structures are subjected to flexure. Conversely, in the case of deep beams where the thickness is not negligible, the Timoshenko model (TBM) [2, 3] is preferable since it assumes a uniform shear distribution along the cross-section of the beam together with the effects of rotatory inertia. However, according to Novozhilov [4], the analysis of thin-walled, open section beams may require more sophisticated theories to achieve sufficiently accurate results.

Over the last century, many refined beam theories have been proposed to overcome the limitation of classical beam modelling. These approaches include the introduction of shear correction factors, the use of warping functions based on de Saint-Venant's solution, the variational asymptotic solution (VABS), the generalized beam theory (GBT), and others. Some selective references and noteworthy contributions are briefly discussed below, with particular attention to dynamic analysis.

Early investigators have focused on the use of appropriate shear corrections factors to increase the accuracy of classical formulations, see for examples Timoshenko and Goodier [5], Sokolniko [6], Stephen [7], and Hutchinson [8]. However, in [9], Jensen showed how the shear correction factor can vary with the natural frequencies. The works by El Fatmi [10, 11, 12] and Ladev  ze et al. [13, 14] are some excellent examples of refined methods based on the use of warping functions. Rand [15] and Kim and White [16] used more or less the same approach in the free vibration analysis by introducing out-of-plane warping with no in-plane stretching terms. Asymptotic type expansion coupled with variational methods has also been proposed by Berdichevsky et al. [17]. Some further valuable contributions are by Volovoi [18], Popescu and Hodges [19], Yu et al. [20], Yu and Hodges [21, 22]. The generalized beam theory (GBT) probably was originated from the work of Schardt [23, 24] and it improves classical beam theories by using piece-wise beam description of thin-walled sections. It has been widely employed and extended in various forms by Silvestre et al. [25, 26] and a dynamic application has been presented by Bebiano et al. [27].

The present work is focused on 1D higher-order theories based on the Carrera Unified Formulation (CUF) to carry out free vibration analysis of solid and thin-walled structures. CUF is well established in the literature for over a decade [28, 29, 30, 31] and it is a hierarchical formulation that considers the order of the model,  $N$ , as a free-parameter (i.e. as an input) of the analysis or in other words,

refined models are obtained without having the need for any ad hoc formulations. In the present work, beam theories using CUF are obtained on the basis of Taylor-type expansions (TE). EBBM and TBM can be obtained as particular cases. The strength of CUF TE 1D models in dealing with arbitrary geometries, thin-walled structures and identifying local effects are well known for both static and free-vibration analysis [32, 33, 34, 35, 36].

In majority of the papers on 1D CUF, the finite element method (FEM) has been used to handle arbitrary geometries and loading conditions. In the present work, the extension of Radial Basis Functions (RBFs) method to higher-order 1D CUF models is proposed. The use of alternative methods to the finite elements for the analysis of structures, such as the meshless methods based on collocation with RBFs, is attractive due to the absence of a mesh and the ease of the collocation techniques. In recent years, RBFs method showed excellent accuracy in the interpolation of data and functions. The RBFs method was first used by Hardy [37, 38] for the interpolation of geographical scattered data and later used by Kansa [39, 40] for the solution of partial differential equations. Afterwards, Ferreira successfully applied RBFs to the analysis of beams and plates [41, 42].

In this work, CUF is adopted to automatically build any-order beam theories. Then, the Principle of Virtual Displacements (PVD) is used to derive the differential governing equations and the associated natural boundary conditions for the generic  $N$ -order model. Next, by assuming harmonic oscillation, the equilibrium equations and the natural boundary conditions are formulated in the frequency domain. The resulting system of ordinary differential equations of second order with constant coefficients is subsequently solved by making use of collocation with Wendland's  $C^6$  RBFs [43]. Finally, modal analyses of both solid and thin-walled structures are produced and compared by published literature and solid/shell models from the commercial code MSC Nastran.

## 2 1D Unified Formulation

### 2.1 Preliminaries

The adopted rectangular cartesian coordinate system is shown in Fig. 1. Let us introduce the transposed displacement vector,

$$\mathbf{u}(x, y, z; t) = \left\{ \begin{matrix} u_x & u_y & u_z \end{matrix} \right\}^T \quad (1)$$

The cross-sectional plane of the structure is denoted by  $\Omega$ , and the beam boundaries over  $y$  are  $0 \leq y \leq L$ . In the case of small displacements with respect to a characteristic dimension in the plane of  $\Omega$ , the strain - displacement relations are

$$\boldsymbol{\epsilon} = \mathbf{D} \mathbf{u} \quad (2)$$

where  $\mathbf{D}$  contains linear differential operators. The expressions of this matrix can be found in [31].

Constitutive laws are exploited to obtain stress components to give

$$\boldsymbol{\sigma} = \tilde{\mathbf{C}} \boldsymbol{\epsilon} \quad (3)$$

The matrix  $\tilde{\mathbf{C}}$  is explicitly given in [31] and it contains the material coefficients  $\tilde{C}_{\alpha\beta}$ , which depend on the Young's modulus, Poisson's ratio, and fiber orientation angle in the case of orthotropic material. For the sake of brevity, the expressions for the coefficients  $\tilde{C}_{\alpha\beta}$  are not reported here, but can be found in standard texts, see for example Tsai [44] and Reddy [45].

Within the framework of the CUF, the displacement field  $\mathbf{u}(x, y, z; t)$  can be expressed as

$$\mathbf{u}(x, y, z; t) = F_\tau(x, z) \mathbf{u}_\tau(y; t), \quad \tau = 1, 2, \dots, M \quad (4)$$

where  $F_\tau$  are the functions of the coordinates  $x$  and  $z$  on the cross-section.  $\mathbf{u}_\tau$  is the vector of the *generalized* displacements,  $M$  stands for the number of terms used in the expansion, and the repeated subscript,  $\tau$ , indicates summation. The choice of  $F_\tau$  determines the class of the 1D CUF model that is required and subsequently to be adopted. TE (Taylor expansion) 1D CUF models consists of a Maclaurin series that uses the 2D polynomials  $x^i z^j$  as base of the  $F_\tau$  functions, where  $i$  and  $j$  are positive integers. For instance, the displacement field of the second-order ( $N = 2$ ) TE model can be expressed as

$$\begin{aligned} u_x &= u_{x_1} + x u_{x_2} + z u_{x_3} + x^2 u_{x_4} + xz u_{x_5} + z^2 u_{x_6} \\ u_y &= u_{y_1} + x u_{y_2} + z u_{y_3} + x^2 u_{y_4} + xz u_{y_5} + z^2 u_{y_6} \\ u_z &= u_{z_1} + x u_{z_2} + z u_{z_3} + x^2 u_{z_4} + xz u_{z_5} + z^2 u_{z_6} \end{aligned} \quad (5)$$

The order  $N$  of the expansion is set as an input option of the analysis; the integer  $N$  is arbitrary and defines the order the beam theory.

An important feature of TE 1D CUF models is that classical beam theories can be obtained as

special cases. For instance, the Timoshenko beam model (TBM) can be realised by using a suitable  $F_7$  expansion. Two conditions have to be imposed: (1) a first-order ( $N = 1$ ) approximation kinematic field:

$$\begin{aligned} u_x &= u_{x1} + x u_{x2} + z u_{x3} \\ u_y &= u_{y1} + x u_{y2} + z u_{y3} \\ u_z &= u_{z1} + x u_{z2} + z u_{z3} \end{aligned} \quad (6)$$

(2) the displacement components  $u_x$  and  $u_z$  have to be constant above the cross-section:

$$u_{x2} = u_{x3} = u_{y2} = u_{y3} = u_{z2} = u_{z3} = 0 \quad (7)$$

Classical theories and first-order models ( $N = 1$ ) require the necessary assumption of reduced material stiffness coefficients to correct Poisson's locking (see [46]). In this paper, Poisson's locking is corrected according to the method outlined by Carrera et al. [31], where further details about TE models can be found.

## 2.2 Governing equations of the N-order TE model

The principle of virtual displacements is used to derive the equations of motion.

$$\delta L_{\text{int}} = \int_V \delta \boldsymbol{\epsilon}^T \boldsymbol{\sigma} dV = -\delta L_{\text{ine}} \quad (8)$$

where  $L_{\text{int}}$  stands for the strain energy and  $L_{\text{ine}}$  is the work done by the inertial loadings.  $\delta$  stands for the usual virtual variation operator. The virtual variation of the strain energy is rewritten using Eq.s (2), (3) and (4). After integrations by part, Eq. (8) becomes

$$\delta L_{\text{int}} = \int_L \delta \mathbf{u}_\tau^T \mathbf{K}^{\tau s} \mathbf{u}_s dy + \left[ \delta \mathbf{u}_\tau^T \boldsymbol{\Pi}^{\tau s} \mathbf{u}_s \right]_{y=0}^{y=L} \quad (9)$$

where  $\mathbf{K}^{\tau s}$  is the differential stiffness matrix and  $\boldsymbol{\Pi}^{\tau s}$  is the matrix of the natural boundary conditions in the form of  $3 \times 3$  fundamental nuclei. The components of  $\mathbf{K}^{\tau s}$  are provided as follows in the case of isotropic material and they are referred to as  $K_{(ij)}^{\tau s}$ , where  $i$  is the row number ( $i = 1, 2, 3$ ) and  $j$  denotes the column number ( $j = 1, 2, 3$ )

$$\begin{aligned} K_{(11)}^{\tau s} &= E_{\tau, x s, x}^{22} + E_{\tau, z s, z}^{44} - E_{\tau s}^{66} \frac{\partial^2}{\partial y^2}, & K_{(12)}^{\tau s} &= (E_{\tau, x s}^{23} - E_{\tau s, x}^{66}) \frac{\partial}{\partial y}, & K_{(13)}^{\tau s} &= E_{\tau, x s, z}^{12} + E_{\tau, z s, x}^{44} \\ K_{(21)}^{\tau s} &= -(E_{\tau s, x}^{23} - E_{\tau, x s}^{66}) \frac{\partial}{\partial y}, & K_{(22)}^{\tau s} &= E_{\tau, x s, x}^{66} + E_{\tau, z s, z}^{55} - E_{\tau s}^{33} \frac{\partial^2}{\partial y^2}, & K_{(23)}^{\tau s} &= (E_{\tau, z s}^{55} - E_{\tau s, z}^{13}) \frac{\partial}{\partial y} \\ K_{(31)}^{\tau s} &= E_{\tau, z s, x}^{12} + E_{\tau, x s, z}^{44}, & K_{(32)}^{\tau s} &= -(E_{\tau s, z}^{55} - E_{\tau, z s}^{13}) \frac{\partial}{\partial y}, & K_{(33)}^{\tau s} &= E_{\tau, x s, x}^{44} + E_{\tau, z s, z}^{11} - E_{\tau s}^{55} \frac{\partial^2}{\partial y^2} \end{aligned} \quad (10)$$

The generic term  $E_{\tau,\theta s,\zeta}^{\alpha\beta}$  above is a cross-sectional moment parameter

$$E_{\tau,\theta s,\zeta}^{\alpha\beta} = \int_{\Omega} \tilde{C}_{\alpha\beta} F_{\tau,\theta} F_{s,\zeta} d\Omega \quad (11)$$

The suffix after the comma in Eq. (10) denotes the derivatives. As far as the natural boundary conditions are concerned, the components of  $\mathbf{\Pi}^{\tau s}$  are

$$\begin{aligned} \Pi_{(11)}^{\tau s} &= E_{\tau s}^{66} \frac{\partial}{\partial y}, & \Pi_{(12)}^{\tau s} &= E_{\tau s,x}^{66}, & \Pi_{(13)}^{\tau s} &= 0 \\ \Pi_{(21)}^{\tau s} &= E_{\tau s,x}^{23}, & \Pi_{(22)}^{\tau s} &= E_{\tau s}^{33} \frac{\partial}{\partial y}, & \Pi_{(23)}^{\tau s} &= E_{\tau s,z}^{13} \\ \Pi_{(31)}^{\tau s} &= 0, & \Pi_{(32)}^{\tau s} &= E_{\tau s,z}^{55}, & \Pi_{(33)}^{\tau s} &= E_{\tau s}^{55} \frac{\partial}{\partial y} \end{aligned} \quad (12)$$

The virtual variation of the inertial work is given by

$$\delta L_{\text{ine}} = \int_L \delta \mathbf{u}_{\tau} \int_{\Omega} \rho F_{\tau} F_s d\Omega \ddot{\mathbf{u}}_s dy = \int_L \delta \mathbf{u}_{\tau} \mathbf{M}^{\tau s} \ddot{\mathbf{u}}_s dy \quad (13)$$

where  $\mathbf{M}^{\tau s}$  is the fundamental nucleus of the mass matrix and double over dots stand as second derivative with respect to time ( $t$ ). The components of matrix  $\mathbf{M}^{\tau s}$  are

$$M_{(11)}^{\tau s} = M_{(22)}^{\tau s} = M_{(33)}^{\tau s} = E_{\tau s}^{\rho} \quad (14)$$

$$M_{(12)}^{\tau s} = M_{(13)}^{\tau s} = M_{(21)}^{\tau s} = M_{(23)}^{\tau s} = M_{(31)}^{\tau s} = M_{(32)}^{\tau s} = 0$$

where

$$E_{\tau s}^{\rho} = \int_{\Omega} \rho F_{\tau} F_s d\Omega \quad (15)$$

$\rho$  is the material density. The derivation of the fundamental nuclei is not provided in this paper but it can be found in [31] in the case of both weak- and strong-form formulations.

The governing equations of the undamped dynamic problem can be written in the following compact form:

$$\delta \mathbf{u}_{\tau} : \mathbf{K}^{\tau s} \mathbf{u}_s = -\mathbf{M}^{\tau s} \ddot{\mathbf{u}}_s \quad (16)$$

Letting  $\mathbf{P}_{\tau}(y; t) = \left\{ \begin{matrix} P_{x\tau} & P_{y\tau} & P_{z\tau} \end{matrix} \right\}^T$  to be the vector of the generalized forces applied at the ends of the beam, the natural boundary conditions are

$$\delta \mathbf{u}_{\tau} : \mathbf{P}_s = \mathbf{\Pi}^{\tau s} \mathbf{u}_s \quad (17)$$



For a fixed theory order  $N$ , Eq.s (16) and (17) have to be expanded using the indices  $\tau$  and  $s$  in order to obtain the governing differential equations and the natural boundary conditions of the desired model.

In the case of harmonic motion, the solution of Eq. (16) is sought in the form

$$\mathbf{u}_s(y; t) = \mathbf{U}_s(y) e^{i\omega t} \quad (18)$$

where  $\mathbf{U}_s(y)$  is the amplitude function of the motion,  $\omega$  is an arbitrary circular or angular frequency, and  $i$  is  $\sqrt{-1}$ . Equation (18) allows the formulation of the differential equilibrium equations and the natural boundary conditions in the frequency domain. Equations (16) and (17) can be rewritten as follows:

$$\delta \mathbf{U}_\tau : (\mathbf{K}^{\tau s} - \omega^2 \mathbf{M}^{\tau s}) \mathbf{U}_s = 0 \quad (19)$$

$$\delta \mathbf{U}_\tau : \bar{\mathbf{P}}_s = \mathbf{\Pi}^{\tau s} \mathbf{U}_s \quad (20)$$

In Eq. (20) the load  $\mathbf{P}_\tau(y; t)$  has been assumed harmonic with amplitude equal to  $\bar{\mathbf{P}}_\tau(y)$ .

### 3 The Radial Basis Functions Method

Radial basis functions (RBFs) approximations are collocation schemes that can exploit accurate representations of the boundary, are easy to implement and can be spectrally accurate. In the framework of the RBFs method, the amplitude of the harmonically varying generalized displacement  $\mathbf{U}_s(y)$  is approximated with a linear combination of the radial basis functions  $\phi_i$ .

$$\mathbf{U}_s(y) = \alpha_{si} \phi_i(\|y - y_i\|_2), \quad i = 1, \dots, n \quad (21)$$

where  $y_i$  is a finite set of  $n$  distinct points (centers) and  $\|y - y_i\|_2$  is the Euclidian distance  $r_i$ , which in the case of 1D problems corresponds to  $|y - y_i|$ . In Eq. (21), index  $i$  indicates summation. Derivatives of  $\mathbf{U}_s(y)$  over  $y$  can be treated similarly.

$$\begin{aligned} \mathbf{U}_{s,y}(y) &= \alpha_{si} \phi_{i,y}(|y - y_i|), & i &= 1, \dots, n \\ \mathbf{U}_{s,yy}(y) &= \alpha_{si} \phi_{i,yy}(|y - y_i|), & i &= 1, \dots, n \end{aligned} \quad (22)$$

In the present paper a Chebyshev grid distribution of points  $y_i$  is used, which is known to be the best choice in terms of stability (see for example [47, 48, 49]).

$$y_i = \frac{L}{2} \left[ 1 - \cos \left( \frac{i-1}{n-1} \pi \right) \right], \quad i = 1, \dots, n \quad (23)$$

Several RBFs have been formulated over the years and they are covered in a large literature. In the present paper, locally supported Wendland's  $C^6$  functions [43] are chosen as  $\phi_i$

$$\phi_i(r_i, c) = \max((1 - cr_i)^8, 0) + (32c^3r_i^3 + 25c^2r_i^2 + 8cr_i + 1) \quad (24)$$

where  $c$  is a positive shape parameter. The shape parameter  $c$  is known to play a very important role in collocation with RBFs for approximating functions and solving partial differential equations, see for example [50, 51]. The accuracy of the solution can vary significantly depending on the choice of the shape parameter indeed. In the literature, several solutions for the evaluation of an optimal value of  $c$  have been proposed depending upon the number of nodes, the distance between the nodes and the type of the RBFs. For instance, in [52] a shape parameter inversely proportional to the square root of the number of grid points was proposed in the case of multiquadrics RBFs. However, finding a good value of the parameter  $c$  is not always an easy task. As specified in [53], smaller values of  $c$  generally lead to higher accuracy. On the other hand, instable numerical solutions may occur as the value of  $c$  is decreased (see [54]). In the present paper, a constant value of  $c$  is used and no optimization procedures are employed. An optimization technique, such as the one recently introduced by Fantuzzi et al. [55], will be the subject of future work.

### 3.1 From a differential problem to a eigenvalue problem via RBFs

Let the domain of the problem be denoted by  $\Gamma$  and let  $\partial\Gamma$  be its boundary. We consider  $n_I$  nodes in  $\Gamma$  and  $n_B$  nodes on  $\partial\Gamma$ , with  $n = n_I + n_B$ . In the particular case of 1D beam theories as in this paper,  $n_B = 2$  (i.e. the two ends of the beam). By substituting Eq.s (21) and (22) into Eq. (19), the differential equations of motion are reduced to a classical eigenvalue problem. For a node  $y_j \in \Gamma$ , it reads:

$$(\mathcal{K}^{\tau sij} - \omega^2 \mathcal{M}^{\tau sij}) \alpha_{si} = 0 \quad (25)$$

where  $\mathcal{K}^{\tau sij}$  and  $\mathcal{M}^{\tau sij}$  are the  $3 \times 3$  fundamental nuclei which contains the coefficients of the algebraic equations of motion. The components of matrix  $\mathcal{K}^{\tau sij}$  are

$$\begin{aligned}
\mathcal{K}_{(11)}^{\tau sij} &= -E_{\tau s}^{66}\phi_{ij,yy} + (E_{\tau,xs}^{22} + E_{\tau,zs,z}^{44})\phi_{ij}, & \mathcal{K}_{(12)}^{\tau sij} &= (E_{\tau,xs}^{23} - E_{\tau s,x}^{66})\phi_{ij,y} \\
\mathcal{K}_{(13)}^{\tau sij} &= (E_{\tau,zs,x}^{44} + E_{\tau,xs,z}^{12})\phi_{ij}, & \mathcal{K}_{(21)}^{\tau sij} &= (E_{\tau,xs}^{66} - E_{\tau s,x}^{23})\phi_{ij,y} \\
\mathcal{K}_{(22)}^{\tau sij} &= -E_{\tau s}^{33}\phi_{ij,yy} + (E_{\tau,xs}^{66} + E_{\tau,zs,z}^{55})\phi_{ij}, & \mathcal{K}_{(23)}^{\tau sij} &= (E_{\tau,zs}^{55} - E_{\tau s,z}^{13})\phi_{ij,y} \\
\mathcal{K}_{(31)}^{\tau sij} &= (E_{\tau,xs,z}^{44} + E_{\tau,zs,x}^{12})\phi_{ij}, & \mathcal{K}_{(32)}^{\tau sij} &= (E_{\tau,zs}^{13} - E_{\tau s,z}^{55})\phi_{ij,y} - E_{\tau s}^{55}\phi_{ij,yy} \\
\mathcal{K}_{(33)}^{\tau sij} &= -E_{\tau s}^{55}\phi_{ij,yy} + (E_{\tau,xs}^{44} + E_{\tau,zs,z}^{11})\phi_{ij}
\end{aligned} \tag{26}$$

The components of matrix  $\mathcal{M}^{\tau sij}$  are

$$\mathcal{M}_{(11)}^{\tau sij} = \mathcal{M}_{(22)}^{\tau sij} = \mathcal{M}_{(33)}^{\tau sij} = E_{\tau s}^p \phi_{ij} \tag{27}$$

$$\mathcal{M}_{(12)}^{\tau sij} = \mathcal{M}_{(13)}^{\tau sij} = \mathcal{M}_{(21)}^{\tau sij} = \mathcal{M}_{(23)}^{\tau sij} = \mathcal{M}_{(31)}^{\tau sij} = \mathcal{M}_{(32)}^{\tau sij} = 0$$

In Eq.s (26) and (27),  $\phi_{ij}$  stands for  $\phi_i(|y_j - y_i|)$ . For a given theory order  $N$ , the eigenvalue problem describing the motion of the beam in free vibration is obtained by expanding  $\mathcal{K}^{\tau sij}$  and  $\mathcal{M}^{\tau sij}$  for  $\tau = 1, 2, \dots, (N+1)(N+2)/2$ ,  $s = 1, 2, \dots, (N+1)(N+2)/2$ ,  $i = 1, \dots, n$ , and  $j = 1, \dots, n_I$ .

$$(\mathcal{K}^I - \omega^2 \mathcal{M}^I) \alpha = 0 \tag{28}$$

where the superscript  $I$  denotes the fact that Eq. (28) applies in  $\Gamma$ . In a similar way, the natural boundary conditions can be written in algebraic form by substituting Eq.s (21) and (22) into Eq. (20).

For a node  $y_j \in \partial\Gamma$ , it reads:

$$\bar{\mathbf{P}}_{sj} = \mathcal{B}^{\tau sij} \alpha_{si} \tag{29}$$

where the components of the fundamental nucleus  $\mathcal{B}^{\tau sij}$  are as follows:

$$\begin{aligned}\mathcal{B}_{(11)}^{\tau sij} &= E_{\tau s}^{66} \phi_{ij,y}, \quad \mathcal{B}_{(12)}^{\tau sij} = E_{\tau s,x}^{66} \phi_{ij}, \quad \mathcal{B}_{(13)}^{\tau sij} = 0 \\ \mathcal{B}_{(21)}^{\tau sij} &= E_{\tau s,x}^{23} \phi_{ij}, \quad \mathcal{B}_{(22)}^{\tau sij} = E_{\tau s}^{33} \phi_{ij,y}, \quad \mathcal{B}_{(23)}^{\tau sij} = E_{\tau s,z}^{13} \phi_{ij} \\ \mathcal{B}_{(31)}^{\tau sij} &= 0, \quad \mathcal{B}_{(32)}^{\tau sij} = E_{\tau s,z}^{55} \phi_{ij}, \quad \mathcal{B}_{(33)}^{\tau sij} = E_{\tau s}^{55} \phi_{ij,y}\end{aligned}\tag{30}$$

For a given expansion order  $N$ , the natural boundary conditions can be obtained in the form of Eq. (31) by expanding  $\mathcal{B}^{\tau sij}$  for  $\tau = 1, 2, \dots, (N+1)(N+2)/2$ ,  $s = 1, 2, \dots, (N+1)(N+2)/2$ ,  $i = 1, \dots, n$ , and  $j = n_I + 1, \dots, n$ . In the case of homogeneous natural boundary condition one has

$$\mathcal{B}^B \alpha = 0\tag{31}$$

where superscript  $B$  denotes the fact that Eq. (31) applies on  $\partial\Gamma$ . Matrix  $\mathcal{B}^B$  is not derived in this paper in the case of essential boundary conditions for the sake of brevity. Essential boundary conditions can be applied by imposing a certain value to the amplitude of the harmonically varying generalized displacement  $\mathbf{U}_s(y) = \overline{\mathbf{U}}_s(y)$ .

Once matrices  $\mathcal{K}^I$ ,  $\mathcal{M}^I$ , and  $\mathcal{B}^B$  are obtained, the final eigenvalue problem can be solved

$$\left( \begin{bmatrix} \mathcal{K}^I \\ \mathcal{B}^B \end{bmatrix} - \omega_k^2 \begin{bmatrix} \mathcal{M}^I \\ \mathbf{0} \end{bmatrix} \right) \alpha_k = 0\tag{32}$$

where  $\alpha_k$  is the  $k$ -th eigenvector. It is well known that some RBFs produces ill-conditioned matrices and this problem increases as the number of grid points rises. Some authors reduce the conditioning number by using preconditioners, see [56]. Moreover, the present work shows that, increasing the expansion order  $N$ , the problem can be severely ill-conditioned. However, scaling the matrices  $\mathcal{K}^I$  and  $\mathcal{M}^I$  as well as the matrix of natural (not essential) boundary conditions  $\mathcal{B}^B$  by the maximum coefficient of the stiffness matrix itself, was sufficient to obtain a well-conditioned problem for each case considered. Nevertheless, in order to further improve the accuracy of the solution, the generalized displacements on the boundary centers could be condensed with respect to those on the internal nodes, as presented in [57].

## 4 Numerical Results

A number of structural problems were considered and the results are discussed in this section. First, free vibration of beams with square cross-section are addressed. Both opened and closed thin-walled structures are subsequently considered so as to show the higher-order capabilities of the present models. The results by the present RBFs method are compared with reference solutions from the literature together with the results obtained from the finite element commercial code MSC Nastran. In all the results below, we use a constant shape parameter  $c = \frac{2.4}{L}$ , where  $L$  is the length of the beam. Our numerical experience shows that this value of the shape parameter produces accurate results. However, the use of an optimization technique will be the subject of a forthcoming work.

### 4.1 Square cross-section

A beam with the cross-section shown in Fig. 2 is considered as the first assessment. The cross-section is square with sides  $b = h = 0.2$  m. The structure is made of an aluminium alloy with Young's modulus  $E$  equal to 75 GPa, Poisson's ratio  $\nu = 0.33$ , and density  $\rho = 2700$  Kg/m<sup>3</sup>.

First the influence of the number of nodes is investigated. Fig. 3 shows the first bending and torsional natural frequencies versus the number of collocation points for the second-order ( $N = 2$ ) model of a clamped-free (CF) beam with length-to-height ratio,  $L/h$ , equal to 10. In Fig. 3, the natural periods computed through the present RBFs method are compared to the exact solution from [36] and they are given in non-dimensional form.

$$\omega^* = \frac{\omega L^2}{h} \sqrt{\frac{\rho}{E}} \quad (33)$$

Good solutions are found by using 37 points, which is the value of  $n$  used in the following analyses.

Table 1 shows the first two bending and torsional natural frequencies for the same beam considered in the convergence study above. Classical TBM and up-to-fifth-order ( $N = 5$ ) refined beam models are addressed. The results by the present CUF-RBFs models are compared to exact refined CUF beam solutions from [36] and a MSC Nastran FE solid model, which is referred to as NAS3D. The NAS3D model was constructed by using a mesh of  $24 \times 24 \times 24$  8-node CHEXA solid elements. In [36, 58, 58], the Dynamic Stiffness Method (DSM) was used to solve in exact form the equations of motion of CUF beam models. However, the main drawback of the DSM is that it results in a transcendental non-linear eigenvalue problem and iterative algorithms (e.g. Wittrick-Williams algorithm) are needed. On the other hand, the proposed RBFs method results in a common linear

eigenvalue problem, whose resolution is extremely fast. Figure 4 shows the modes under consideration according to the fifth-order CUF-RBFs model ( $N = 5$ ).

The results by CUF beam models are in good agreement with the MSC Nastran 3D elasticity FEM model. It is additionally shown that RBFs gives good results when applied to 1D CUF models. Although the shape parameter  $c$  is known from the literature to be dependant on the geometrical and mechanical properties of the problem, it is shown in the present analysis that, once the shape parameter  $c$  has been chosen, both torsional and bending modes exhibit a good convergence versus the number of collocation points  $n$ . Moreover, the results show that for the problem considered good results are obtained for a value of  $c$  equal to  $\frac{2.4}{L}$ , which is demonstrated to be independent on the expansion order of the beam theory.

## 4.2 Open thin-walled beams

A beam with a C-shaped cross-section is addressed as the second example. The geometry of the cross-section is shown in Fig. 5. The beam has sides  $b = h = 0.2$  m and length-to-side ratio  $L/h = 10$ , whereas the thickness of the flanges is  $t = 0.02$  m. The structure is made of a steel alloy with the following characteristics:  $E = 198$  GPa,  $\nu = 0.3$ ,  $\rho = 7850$  Kg/m<sup>3</sup>.

Good solutions were found for the C-shaped beam with  $c = \frac{2.4}{L}$  and  $n = 33$ , and the results are given in Table 2 for clamped-clamped (CC) boundary conditions. In Table 2 the first 10 modes are considered together with the number of the degrees of freedom (DOFs) for each model, and the results by the present method are compared with the results by 1D, 2D, and 3D MSC Nastran FE models. In particular, the model denoted as NAS1D in column 9, was obtained by using 50 CBAR beam elements. The NAS2D model was constructed by using 3000 4-node CQUAD MSC Nastran plate elements, whereas the NAS3D model was made of 112 8-node CHEXA solid elements on the cross-section with aspect-ratio equal to 2. In Table 2, columns 2 to 8 quotes the results by classical TBM to eight-order ( $N = 8$ ) beam models obtained with the present RBFs method. Figure 6 shows some selected modes of the C-shaped beam by the present eight-order ( $N = 8$ ) 1D CUF model.

The shown results clearly demonstrate the efficiency of the present models, which are able to deal with shell- and solid-like phenomena with a very low number of DOFs. It is clear that higher-order models are able to deal with torsional, local shell-like as well as coupling effects in accordance with NAS2D and NAS3D models. On the other hand, classical and lower-order beam models are sufficient to characterize pure bending modes (e.g. Mode 2). It is further shown that the present RBFs method gives good accuracy and stability when applied to higher-order models, even if very

high expansion orders are considered. Instability problems only occurred when considering higher than eight-order models. Nevertheless, an optimization procedure of the shape parameter  $c$  - which is considered to be constant and equal to  $\frac{2.4}{L}$  in the present paper - could give us the possibility to further enrich the displacement field so that to enhance the solution.

The thin-walled Z-shaped cross-section of Fig. 7 is further considered. The height of the cross-section is  $h = 0.3$  m, whereas the length of each horizontal flange is equal to  $b = 0.2$  m. The thickness of both the flanges and the vertical web is  $t = 0.005$  m. The beam is subjected to clamped-free (CF) boundary conditions and it has length equal to 3 m. A homogeneous steel alloy with  $E = 206$  GPa,  $\nu = 0.3$ , and  $\rho = 7800$  Kg/m<sup>3</sup> is considered for this problem.

The first natural frequencies for each model implemented are shown in Table 3, where also the number of DOFs is given. In Table 3 the natural frequencies related to the first bending, the first torsional, and the first two local flanges modes are given and the results by the present methodology are compared with those from a 2D MSC Nastran model made by 5251 4-node CQUAD elements. The mode shapes by the present eight-order  $N = 8$  beam model are shown in Fig. 8.

The results provided by the present CUF beam models were obtained by using  $c = \frac{2.4}{L}$  and  $n = 33$ . The analysis once again highlights the capability of the present beam theories to deal with higher-order and localized phenomena. In fact, results in good agreement with NAS2D model were found with very low DOFs. As in the previous analysis case, better results could be found by further increasing the expansion order  $N$  but this would require appropriate optimization techniques of the RBFs shape parameter.

### 4.3 Thin-walled cylinder

A thin-walled cylinder is considered as the final example to further highlight the higher-order capabilities of the present formulation. The cross-section geometry is shown in Fig. 9. The cylinder has the outer diameter  $d$  equal to 2 m, thickness  $t = 0.02$  m, and length  $L = 20$  m. The structure is made of the same metallic material as in the first example, i.e.  $E = 75$  GPa,  $\nu = 0.33$ , and  $\rho = 2700$  Kg/m<sup>3</sup>. For the problem under consideration a number of points  $n$  equal to 31 was used along the  $y$ -axis direction.

Table 4 show the natural frequencies of the thin-walled cylinder for different boundary conditions. In particular, free-free (FF), clamped-free (CF), clamped-clamped (CC), as well as simply-supported (SS) ends were considered. Both classical TBM and higher-order CUF beam models are shown in Table 4, where the results by the present RBFs-based method are compared to exact higher-order

beam models and MSC Nastran 2D FE shell solutions from [36]. It is shown that classical and lower-order beam models are able to capture bending and torsional modes, whereas 1D higher-order theories are mandatory in order to detect local shell-like modes in accordance with 2D solutions.

Figure 10 shows the percentage error between the present RBFs method and exact reference solution from [36]. In Fig. 10 the first bending, torsional, and shell-like modes for different expansion orders  $N$  and boundary conditions are considered. It is shown that, for fixed values of the parameters  $c$  and  $n$ , bending and torsional modes exhibit a good convergence for all the boundary conditions and theory order considered. On the other hand, shell-like modes become instable if higher than fourth-order ( $N = 4$ ) models and  $CF$  or  $FF$  boundary conditions are examined. This is the reason why in Table 4 only up to  $N = 4$  models are considered for those boundary conditions. However, the authors are confident that an optimization procedure on parameters  $c$  and  $n$  will overcome the issue.

To conclude, Fig. 11 shows the first two bending, shell-like, and torsional mode shapes of the cylinder with  $CC$  boundary conditions in order to further underline the 3D capabilities of the present theories.

## 5 Conclusions

An higher-order beam formulation has been developed by using the CUF, which allows for the formulation of any-order beam theories by setting the expansion order as an input of the analysis. Numerical results have been obtained and the differential equations of motion solved through RBFs collocation method. Wendlands  $C^6$  RBFs has been used to approximate the generalized displacements and their derivatives along the beam axis. A shape parameter inversely proportional to the beam length has been used. Compact as well as open and closed thin-walled sections have been analyzed and the results compared with those obtained using MSC Nastran FEM models and with those from the literature. It is shown that accurate and computationally efficient results can be obtained by coupling CUF with RBFs method. The proposed study also shows that the choice of the RBFs shape parameter can have a non-negligible influence on the accuracy of the solution. However, the investigation provides optimism for future studies of techniques aiming in the optimization of the shape parameter depending on the geometry, on the boundary condition, as well as on the expansion order of the beam theory.



## References

- [1] L. Euler. *De curvis elasticis*. Lausanne and Geneva: Bousquet, 1744. (English translation: W. A. Oldfather, C. A. Elvis, D. M. Brown, Leonhard Euler's elastic curves, *Isis* 20 (1933) 72–160).
- [2] S. P. Timoshenko. On the corrections for shear of the differential equation for transverse vibrations of prismatic bars. *Philosophical Magazine*, 41:744–746, 1922.
- [3] S. P. Timoshenko. On the transverse vibrations of bars of uniform cross section. *Philosophical Magazine*, 43:125–131, 1922.
- [4] V. V. Novozhilov. *Theory of elasticity*. Pergamon, Elmsford, 1961.
- [5] S. P. Timoshenko and J. N. Goodier. *Theory of elasticity*. McGraw-Hill, 1970.
- [6] I. S. Sokolnikoff. *Mathematical theory of elasticity*. McGraw-Hill, 1956.
- [7] N. G. Stephen. Timoshenko's shear coefficient from a beam subjected to gravity loading. *Journal of Applied Mechanics*, 47:121–127, 1980.
- [8] J. R. Hutchinson. Shear coefficients for Timoshenko beam theory. *Journal of Applied Mechanics*, 68:87–92, 2001.
- [9] J. J. Jensen. On the shear coefficient in Timoshenko's beam theory. *Journal of Sound and Vibration*, 87(4):621–635, 1983.
- [10] R. El Fatmi. On the structural behavior and the Saint Venant solution in the exact beam theory: application to laminated composite beams. *Computers and Structures*, 80(16–17):1441–1456, 2002.
- [11] R. El Fatmi. Non-uniform warping including the effects of torsion and shear forces. Part I: a general beam theory. *International Journal of Solids and Structures*, 44(18–19):5912–5929, 2007.
- [12] R. El Fatmi. Non-uniform warping including the effects of torsion and shear forces. Part II: analytical and numerical applications. *International Journal of Solids and Structures*, 44(18–19):5930–5952, 2007.
- [13] P. Ladéveze and J. Simmonds. New concepts for linear beam theory with arbitrary geometry and loading. *European Journal Of Mechanics A/Solids*, 17(3):377–402, 1998.

- [14] P. Ladéveze, P. Sanchez, and J. Simmonds. Beamlike (Saint-Venant) solutions for fully anisotropic elastic tubes of arbitrary closed cross-section. *International Journal of Solids and Structures*, 41(7):1925–1944, 2004.
- [15] O. Rand. Free vibration of thin-walled composite blades. *Composite Structures*, 28:169–180, 1994.
- [16] C. Kim and S. R. White. Thick-walled composite beam theory including 3-D elastic effects and torsional warping. *International Journal of Solids and Structures*, 34(31–32):4237–4259, 1997.
- [17] V. L. Berdichevsky, E. Armanios, and A. Badir. Theory of anisotropic thin-walled closed-cross-section beams. *Composites Engineering*, 2(5–7):411–432, 1992.
- [18] V. V. Volovoi, D. H. Hodges, V. L. Berdichevsky, and V. G. Sutyrin. Asymptotic theory for static behavior of elastic anisotropic I-beams. *International Journal of Solids and Structures*, 36:1017–1043, 1999.
- [19] B. Popescu and D. H. Hodges. On asymptotically correct Timoshenko-like anisotropic beam theory. *International Journal of Solids and Structures*, 37:535–558, 2000.
- [20] W. Yu, V. V. Volovoi, D. H. Hodges, and X. Hong. Validation of the variational asymptotic beam sectional analysis (VABS). *AIAA Journal*, 40:2105–2113, 2002.
- [21] W. Yu and D. H. Hodges. Elasticity solutions versus asymptotic sectional analysis of homogeneous, isotropic, prismatic beams. *Journal of Applied Mechanics*, 71:15–23, 2004.
- [22] W. Yu and D. H. Hodges. Generalized Timoshenko theory of the variational asymptotic beam sectional analysis. *Journal of the American Helicopter Society*, 50(1):46–55, 2005.
- [23] R. Schardt. Eine erweiterung der technischen biegetheorie zur berechnung prismatischer faltwerke (Extension of the engineer’s theory of bending to the analysis of folded plate structures). *Der Stahlbau*, 35:161–171, 1966.
- [24] R. Schardt. Generalized beam theory an adequate method for coupled stability problems. *Thin-Walled Structures*, 19:161–180, 1994.
- [25] N. Silvestre and D. Camotim. First-order generalised beam theory for arbitrary orthotropic materials. *Thin-Walled Structures*, 40(9):755–789, 2002.

- [26] N. Silvestre. Second-order generalised beam theory for arbitrary orthotropic materials. *Thin-Walled Structures*, 40(9):791–820, 2002.
- [27] R. Bebbiano, N. Silvestre, and D. Camotim. Local and global vibration of thin-walled members subjected to compression and non-uniform bending. *Journal of Sound and Vibration*, 345:509–535, 2008.
- [28] E. Carrera. A class of two dimensional theories for multilayered plates analysis. *Atti Accademia delle Scienze di Torino, Memorie Scienze Fisiche*, 19-20:49–87, 1995.
- [29] E. Carrera. Theories and finite elements for multilayered, anisotropic, composite plates and shells. *Archives of Computational Methods in Engineering*, 9(2):87–140, 2002.
- [30] E. Carrera. Theories and finite elements for multilayered plates and shells: a unified compact formulation with numerical assessment and benchmarking. *Archives of Computational Methods in Engineering*, 10(3):216–296, 2003.
- [31] E. Carrera, G. Giunta, and M. Petrolo. *Beam Structures: Classical and Advanced Theories*. John Wiley & Sons, 2011. DOI: 10.1002/9781119978565.
- [32] E. Carrera, M. Petrolo, and E. Zappino. Performance of CUF approach to analyze the structural behavior of slender bodies. *Journal of Structural Engineering*, 138(2):285–297, 2012. DOI: 10.1061/(ASCE)ST.1943-541X.0000402.
- [33] E. Carrera, M. Petrolo, and P. Nali. Unified formulation applied to free vibrations finite element analysis of beams with arbitrary section. *Shock and Vibrations*, 18(3):485–502, 2011. DOI: 10.3233/SAV-2010-0528.
- [34] E. Carrera, M. Petrolo, and A. Varello. Advanced beam formulations for free vibration analysis of conventional and joined wings. *Journal of Aerospace Engineering*, 25(2):282–293, 2012. DOI: 10.1061/(ASCE)AS.1943-5525.0000130.
- [35] M. Petrolo, E. Zappino, and E. Carrera. Refined free vibration analysis of one-dimensional structures with compact and bridge-like cross-sections. *Thin-Walled Structures*, 56:49–61, 2012. DOI: 10.1016/j.tws.2012.03.011.
- [36] A. Pagani, M. Boscolo, J.R. Banerjee, and E. Carrera. Exact dynamic stiffness elements based on one-dimensional higher-order theories for free vibration analysis of solid and thin-walled structures. *Journal of Sound and Vibration*, 332(23):6104–6127, 2013.

- [37] R. L. Hardy. Multiquadric equations of topography and other irregular surfaces. *Geophysical Research*, 176:1905–1915, 1971.
- [38] R. L. Hardy. Theory and applications of the multiquadric-biharmonic method: 20 years of discovery. *Computers Math. Applic.*, 19(8/9):163–208, 1990.
- [39] E. J. Kansa. Multiquadrics- a scattered data approximation scheme with applications to computational fluid dynamics. i: Surface approximations and partial derivative estimates. *Computers and Mathematics with Applications*, 19(8/9):127–145, 1990.
- [40] E. J. Kansa. Multiquadrics- a scattered data approximation scheme with applications to computational fluid dynamics. ii: Solutions to parabolic, hyperbolic and elliptic partial differential equations. *Computers and Mathematics with Applications*, 19(8/9):147–161, 1990.
- [41] A. J. M. Ferreira. A formulation of the multiquadric radial basis function method for the analysis of laminated composite plates. *Composite Structures*, 59(3):385–392, 2003.
- [42] A. J. M. Ferreira. Thick composite beam analysis using a global meshless approximation based on radial basis functions. *Mechanics of Advanced Materials and Structures*, 10:271–284, 2003.
- [43] H. Wendland. Error estimates for interpolation by compactly supported radial basis functions of minimal degree. *Journal of Approximation Theory*, 93:258–296, 1998.
- [44] S. W. Tsai. *Composites Design*. Dayton, Think Composites, 4th edition, 1988.
- [45] J. N. Reddy. *Mechanics of laminated composite plates and shells. Theory and Analysis*. CRC Press, 2nd edition, 2004.
- [46] E. Carrera and S. Brischetto. Analysis of thickness locking in classical, refined and mixed multilayered plate theories. *Composite Structures*, 82(4):549–562, 2008.
- [47] A.J.M. Ferreira, C.M.C. Roque, and P.A.L.S. Martins. Analysis of composite plates using higher-order shear deformation theory and a finite point formulation based on the multiquadric radial basis function method. *Composites Part B: Engineering*, 34(7):627–636, 2003.
- [48] S. Xiang, Z.-Y. Bi, S.-X. Jiang, Y.-X. Jin, and M.-S. Yang. Thin plate spline radial basis function for the free vibration analysis of laminated composite shells. *Composite Structures*, 93(2):611–615, 2011.

- [49] A.J.M. Ferreira, G.E. Fasshauer, R.C. Batra, and J.D. Rodrigues. Static deformations and vibration analysis of composite and sandwich plates using a layerwise theory and rbf-ps discretizations with optimal shape parameter. *Composite Structures*, 86(4):328–343, 2008.
- [50] C. M. C. Roque and A. J. M. Ferreira. Numerical experiments on optimal shape parameters for radial basis functions. *Numerical Methods for Partial Differential Equations*, 26(3):675–689, 2010.
- [51] W. H. Press, S. A. Teukolsky, W. T. Vetterling, and B. P. Flannery. *Numerical Recipes: The Art of Scientific Computing*. Cambridge University Press, New York, 3rd edition, 2007.
- [52] G. E. Fasshauer. Newton iteration with multiquadrics for the solution of nonlinear pdes. *Comput. Math. Applic.*, 43:423–438, 2002.
- [53] A. J. M. Ferreira and G. E. Fasshauer. Computation of natural frequencies of shear deformable beams and plates by a rbf-pseudospectral method. *Computer Methods in Applied Mechanics and Engineering*, 196:134–146, 2006.
- [54] R. Schaback. On the efficiency of interpolation by radial basis functions. In A. Le Méhauté, C. Rabut, and L. L. Schumaker, editors, *Proceedings of Surface fitting and multiresolution methods*, pages 309–318. Vanderbilt University Press, 1997.
- [55] N. Fantuzzi, F. Tornabene, E. Viola, and A.J.M. Ferreira. A strong formulation finite element method (sfem) based on rbf and gdq techniques for the static and dynamic analyses of laminated plates of arbitrary shape. *Meccanica*, 49(10):2503–2542, 2014.
- [56] E. J. Kansa and Y. C. Hon. Circumventing the ill-conditioning problem with multiquadric radial basis functions. *Computers and Mathematics with Applications*, 39(7–8):123–137, 2000.
- [57] F. Tornabene, N. Fantuzzi, E. Viola, and A.J.M. Ferreira. Radial basis function method applied to doubly-curved laminated composite shells and panels with a general higher-order equivalent single layer formulation. *Composites Part B: Engineering*, 55(0):642–659, 2013.
- [58] A. Pagani, E. Carrera, M. Boscolo, and J.R. Banerjee. Refined dynamic stiffness elements applied to free vibration analysis of generally laminated composite beams with arbitrary boundary conditions. *Composite Structures*, 110(23):305–316, 2014.

## Tables

Model	I Bending	II Bending	I Torsional	II Torsional
MSC Nastran, [36]				
NAS3D	1.016	6.088	8.852	26.516
Reference CUF solutions, [36]				
$N = 5$	1.013	6.069	8.868	26.603
$N = 4$	1.013	6.070	8.871	26.619
$N = 3$	1.014	6.075	9.631	28.893
$N = 2$	1.015	6.107	9.631	28.893
TBM	1.008	6.069	-*	-
Present CUF-RBFs				
$N = 5$	1.011	6.075	8.872	26.605
$N = 4$	1.012	6.078	8.875	26.623
$N = 3$	1.013	6.081	9.634	28.895
$N = 2$	1.014	6.115	9.634	28.895
TBM	1.007	6.076	-	-

\*: not provided by the model

Table 1: First two bending and torsional non-dimensional natural periods for the CF square beam,  $L/h = 10$ ,  $c = \frac{2.4}{L}$ ,  $n = 37$

DOFs	TBM	$N = 1$	$N = 2$	$N = 4$	$N = 6$	$N = 7$	$N = 8$	NAS1D	NAS2D	NAS3D
	165	297	594	1485	2772	3564	4455	298	15345	337305
Mode 1 <sup>b1</sup>	324.575	324.575	326.251	188.454	139.540	134.796	130.659	272.327	120.715	123.035
Mode 2 <sup>b2</sup>	267.018	267.018	268.805	259.464	258.242	257.549	257.052	259.183	253.081	255.122
Mode 3 <sup>b1</sup>	802.476	802.476	805.308	421.352	327.164	317.465	307.669	612.380	273.476	280.688
Mode 4 <sup>f</sup>	-*	-	-	1897.637	495.647	462.566	372.945	-	289.323	297.244
Mode 5 <sup>f</sup>	-	-	-	1919.707	536.076	500.446	417.306	-	331.782	340.822
Mode 6 <sup>f</sup>	-	-	-	1952.249	610.236	568.936	491.753	-	403.791	414.174
Mode 7 <sup>b1</sup>	1408.623	1408.623	1418.413	700.446	540.593	517.619	493.195	1010.938	406.396	420.235
Mode 8 <sup>t</sup>	-	779.002	762.101	491.664	468.266	466.559	465.139	-	460.264	463.815
Mode 9 <sup>f</sup>	-	-	-	2002.983	704.519	659.198	589.383	-	499.572	511.418
Mode 10 <sup>b1</sup>	2088.731	2088.731	2085.379	998.768	734.409	689.258	647.332	1432.700	521.399	539.183

*b1*: Bending (plane  $yz$ )/Flanges mode

*b2*: Bending mode on plane  $xy$

*f*: Flanges mode

*t*: Torsional mode

\*: Mode not provided by the theory

Table 2: Natural frequencies ( $Hz$ ) of the CC C-shaped beam,  $c = \frac{2.4}{L}$ ,  $n = 33$

	TBM	$N = 1$	$N = 2$	$N = 4$	$N = 6$	$N = 7$	$N = 8$	NAS2D
DOFs	165	297	594	1485	2772	3564	4455	27000
Mode 1 <sup>b</sup>	15.261	15.261	15.375	15.306	15.091	15.058	15.048	15.214
Mode 2 <sup>t</sup>	-*	265.748	162.570	38.767	24.763	24.269	24.187	21.247
Mode 3 <sup>f</sup>	-	-	-	250.566	41.035	40.805	40.018	37.893
Mode 4 <sup>f</sup>	-	-	-	505.329	91.971	78.532	66.927	54.559

*b*: Bending mode on plane  $xy$

*t*: Torsional mode

*f*: Flanges mode

\*: Mode not provided by the theory

Table 3: Natural frequencies ( $Hz$ ) of the CF Z-shaped beam,  $c = \frac{2.4}{L}$ ,  $n = 33$

BCs	Model	I Bending	II Bending	I Shell-like	II Shell-like	I Torsional	II Torsional
SS	NAS2D, [36]	13.978	51.366	14.913	22.917	80.415	160.810
	$N = 5$ , Exact [36]	14.022	51.503	18.405	25.460	80.786	161.573
	$N = 5$	14.294	51.567	18.608	25.574	80.639	162.551
	$N = 4$	14.294	51.568	23.656	29.403	80.636	162.692
	$N = 3$	14.295	51.583	35.049	61.353	80.847	161.712
	$N = 2$	14.463	53.648	-*	-	80.838	161.596
	TBM	14.459	53.604	-	-	-	-
CC	NAS2D, [36]	28.498	68.960	17.396	30.225	80.415	160.810
	$N = 5$ , Exact [36]	28.576	69.110	20.484	32.222	80.786	161.573
	$N = 5$	28.354	69.096	20.463	31.974	80.838	161.596
	$N = 4$	28.352	69.097	25.060	34.897	80.838	161.596
	$N = 3$	28.259	68.921	38.889	70.056	80.838	161.596
	$N = 2$	30.742	77.452	-	-	80.838	161.596
	TBM	30.435	76.489	-	-	-	-
CF	NAS2D, [36]	5.059	29.001	14.235	17.435	40.209	120.620
	$N = 4$ , Exact [36]	5.077	29.090	23.069	25.239	40.394	121.181
	$N = 4$	5.047	29.002	23.003	24.979	40.431	121.203
	$N = 3$	5.059	28.953	26.934	49.356	40.431	121.203
	$N = 2$	5.059	30.423	-	-	40.431	121.203
	TBM	5.060	30.312	-	-	-	-
FF	NAS2D, [36]	30.829	76.806	14.129	14.171	80.415	160.810
	$N = 4$ , Exact [36]	30.932	77.043	22.987	23.053	80.789	161.577
	$N = 4$	30.945	77.052	22.864	23.048	80.787	161.592
	$N = 3$	31.121	77.099	23.043	34.678	80.787	161.592
	$N = 2$	31.349	80.346	-	-	80.787	161.592
	TBM	31.341	80.286	-	-	-	-

\*: not provided by the model

Table 4: Natural frequencies ( $Hz$ ) of the thin-walled cylinder for different boundary conditions,  $c = \frac{2.4}{L}$ ,  $n = 31$



## Figures

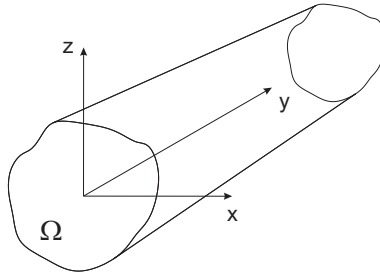


Figure 1: Coordinate frame of the beam model

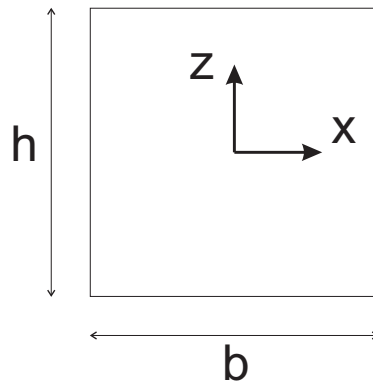
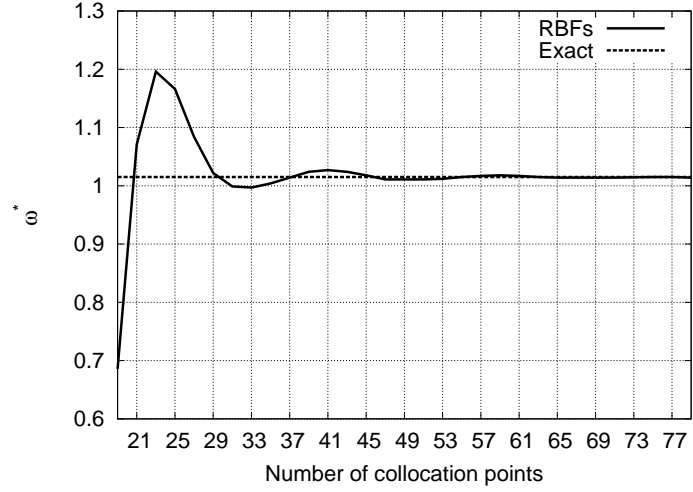
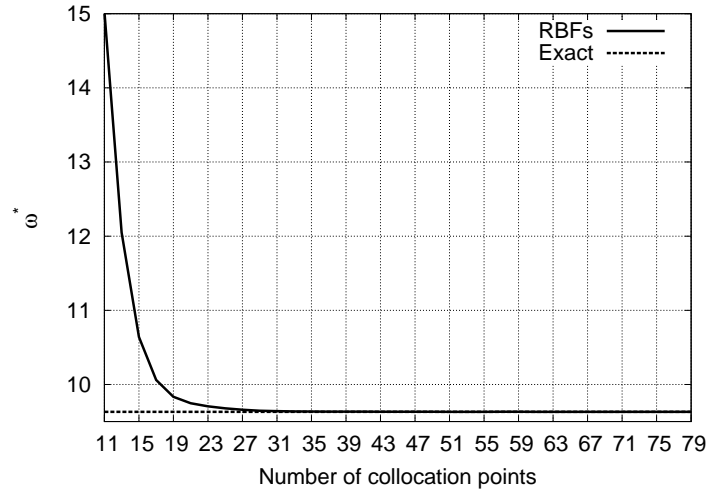


Figure 2: Square cross-section



(a)



(b)

Figure 3: Influence of the number of points,  $n$ , on the first bending (a) and torsional (b) non-dimensional periods for the second-order ( $N = 2$ ) model of the CF rectangular beam

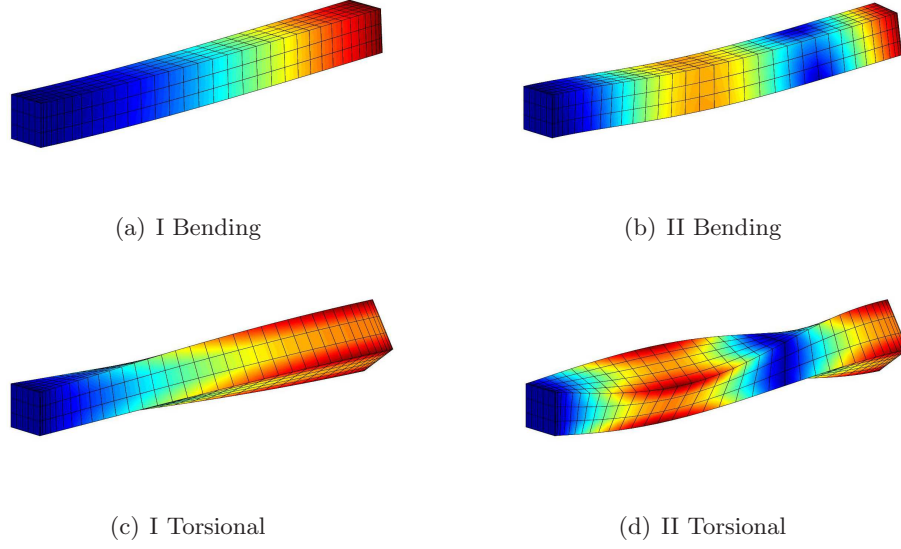


Figure 4: First two bending and torsional modes of the CF rectangular beam,  $N = 5$ ,  $c = \frac{2.4}{L}$ ,  $n = 37$

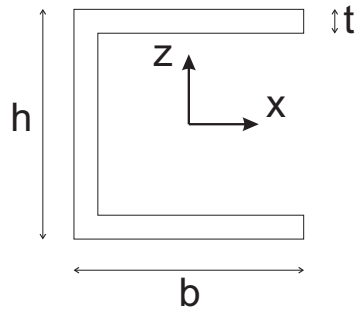


Figure 5: C-shaped cross-section

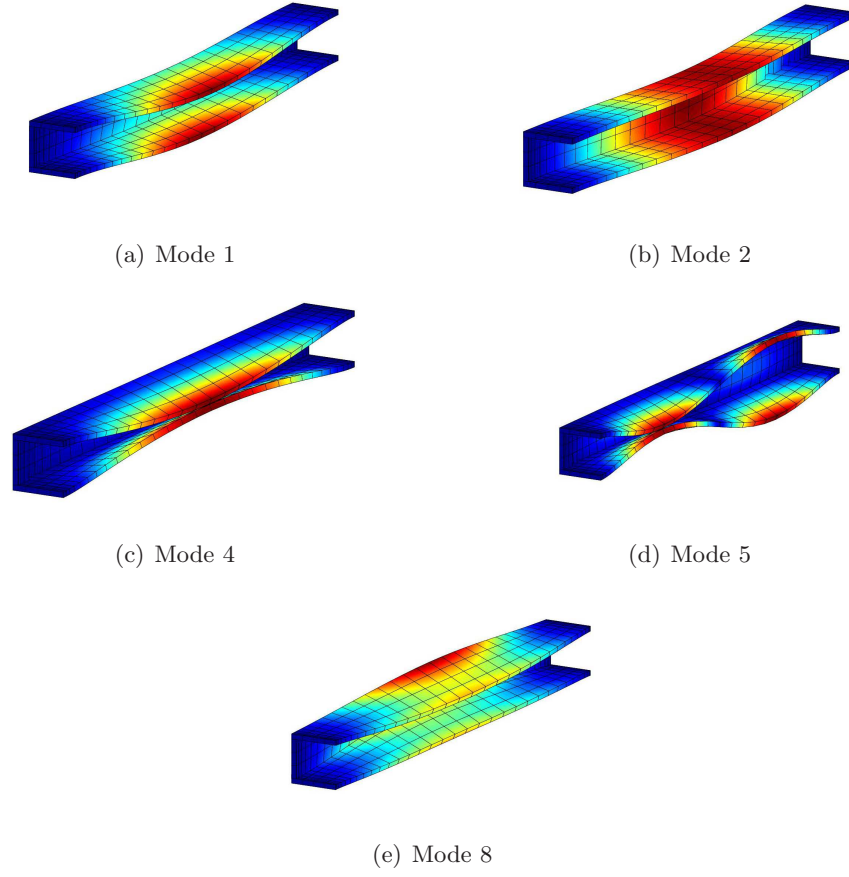


Figure 6: Natural modes of the CC C-shaped beam: (a) Bending (plane  $yz$ )/flanges mode; (b) bending on plane  $xy$ ; (c-d) flanges modes; (e) torsional mode.  $N = 8$ ,  $c = \frac{2.4}{L}$ ,  $n = 33$

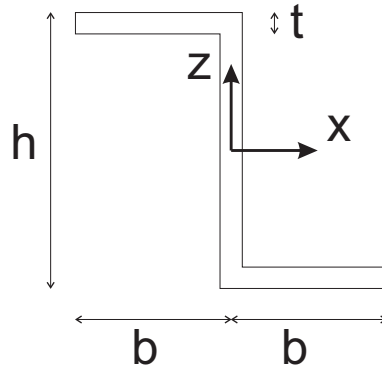


Figure 7: Z-shaped cross-section

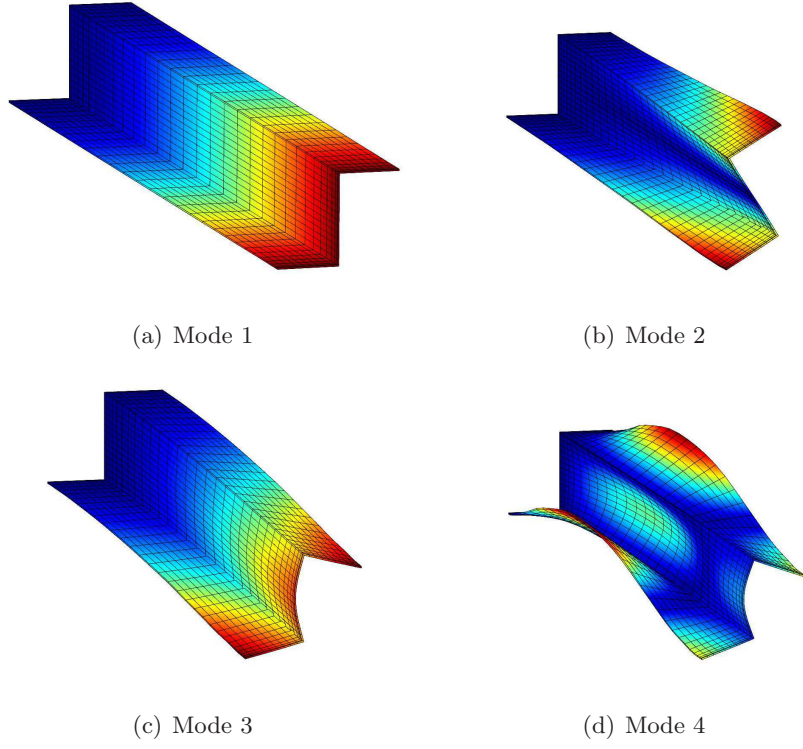


Figure 8: Natural modes of the CF Z-shaped beam: (a) Bending (plane  $xy$ ); (b) torsional; (c-d) flanges modes.  $N = 8$ ,  $c = \frac{2.4}{L}$ ,  $n = 33$

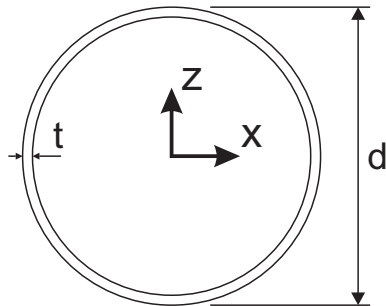


Figure 9: Cross-section of the thin-walled cylinder

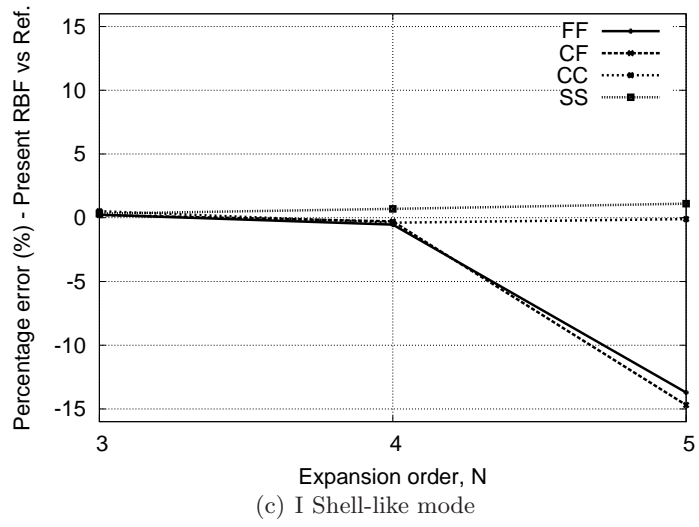
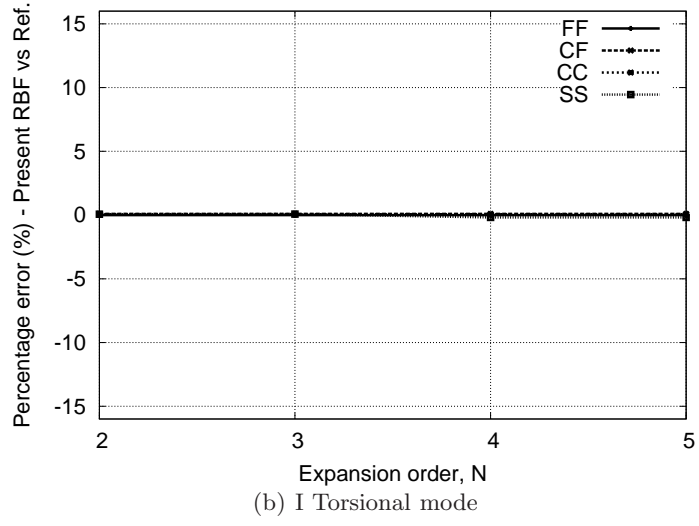
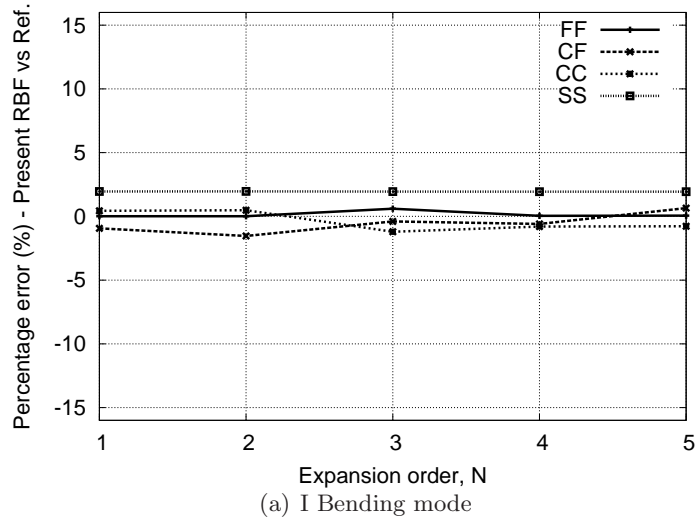
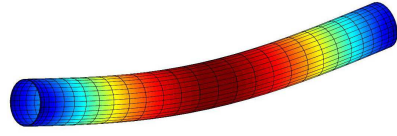
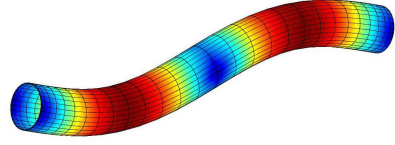


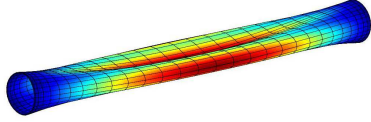
Figure 10: Percentage error between the present RBFs and exact reference solutions [36] for various expansion orders and BCs. Thin-walled cylinder,  $c = \frac{2.4}{L}$ ,  $n = 31$



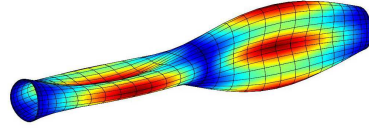
(a) I Bending



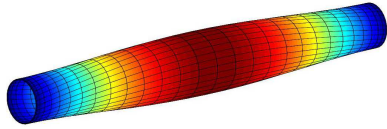
(b) II Bending



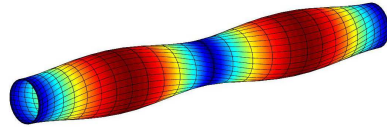
(c) I Shell-like



(d) II Shell-like



(e) I Torsional



(f) II Torsional

Figure 11: First two bending, shell-like, and torsional modes of the SS thin-walled cylinder,  $N = 5$ ,  $c = \frac{2.4}{L}$ ,  $n = 31$